Bead-Fourier path integral molecular dynamics

Sergei D. Ivanov,* Alexander P. Lyubartsev, and Aatto Laaksonen
Division of Physical Chemistry, Arrhenius Laboratory, Stockholm University, S-10691, Stockholm, Sweden
(Received 20 December 2002; published 27 June 2003)

Molecular dynamics formulation of Bead-Fourier path integral method for simulation of quantum systems at finite temperatures is presented. Within this scheme, both the bead coordinates and Fourier coefficients, defining the path representing the quantum particle, are treated as generalized coordinates with corresponding generalized momenta and masses. Introduction of the Fourier harmonics together with the center-of-mass thermostating scheme is shown to remove the ergodicity problem, known to pose serious difficulties in standard path integral molecular dynamics simulations. The method is tested for quantum harmonic oscillator and hydrogen atom (Coulombic potential). The simulation results are compared with the exact analytical solutions available for both these systems. Convergence of the results with respect to the number of beads and Fourier harmonics is analyzed. It was shown that addition of a few Fourier harmonics already improves the simulation results substantially, even for a relatively small number of beads. The proposed Bead-Fourier path integral molecular dynamics is a reliable and efficient alternative to simulations of quantum systems.

DOI: 10.1103/PhysRevE.67.066710 PACS number(s): 02.70.Ns, 31.15.Kb, 05.30.−d

I. INTRODUCTION

Path integral (PI) simulation techniques, based on Feynman path integral formalism [1] provide a powerful tool to study quantum many-body systems. The quantum partition function can be presented as an imaginary-time path integral [1,2], formally equivalent to the configurational integral over closed trajectories, or paths. The PI formalism is exact and straightforward to use for systems of interacting quantum particles but it requires, in principle, an infinite number of parameters to define the trajectory. Therefore, finite-number approximations have to be used to treat the path integrals in numerical computer simulations.

Historically, two main branches of approximative methods have appeared. In the first, so-called discretized or *Bead* approximation [3] scheme the trajectory is represented as a ''ring polymer,'' consisting of a finite number of beads connected together with harmonic springs. Second, the *Fourier* approximation [4] method describes the trajectory by a finite set of Fourier series terms. Further, there exist different variants within the two categories (see, for example, Ref. [5] for Fourier-based approaches). Coalson [6] has shown that, in the high-order implementation, i.e., when the number of parameters representing the trajectory is large, the bead and Fourier approaches are essentially the same. Studies of the relative efficiencies of the different versions of both the methods [5–8] show that the efficiency can vary substantially depending on the particular system and the specific algorithm.

Recently, a combined Bead-Fourier (BF) Monte Carlo (MC) method was suggested by Vorontsov-Velyaminov, Nesvit, and Gorbunov [9] in which the parts of the trajectory between the beads are presented as a Fourier series. It was shown in this paper and in the subsequent works [10,11] that by combining the bead and Fourier contributions in an optimal way, a substantial performance improvement can be obtained in path integral Monte Carlo (PIMC) simulations.

Typically, the Metropolis Monte Carlo algorithm is used to sample the trajectories in PIMC simulations. An alternative way to generate an ensemble of trajectories with a canonical probability distribution is to use molecular dynamics (MD) algorithms with a suitable thermostat [12–15]. One of the reasons of interest to molecular dynamics algorithms is a hope to improve sampling over the configurational space in certain cases: for very light particles, where description requires high numbers of beads, for systems of many identical particles, etc. For instance, in Ref. [15], the path integral molecular dynamics (PIMD) algorithm was applied to describe a solvated electron, a system where several hundred of beads were required.

Another reason for the interest to the PIMD method is that, being formulated as *centroid* dynamics, it can describe real-time dynamics in a semiclassical approximation. The corresponding formalism has been developed by Cao and Voth in a series of works [16–18]. In their formulation the motion of the path centroid (i.e., center of mass of the trajectory) in an effective (mean force) potential is generated by all the beads of the path. Centroid dynamics has been shown to be exact for a harmonic potential and gives a correct classical limit. It has been used in a number of applications [19–22] and also included as an option in the CPMD (Car-Parrinello molecular dynamics) [23] package, now a standard tool in *ab-initio* MD simulations.

The purpose of this work is to present a molecular dynamics approach for simulations of quantum systems based on Bead-Fourier representation of path integrals. We hope that our BF-PIMD approach would help resolve the difficulties experienced in using the standard bead algorithm in cases when the number of required beads rapidly increases, causing the springs, connecting the beads, to become stiffer. Within the MC method this leads to ergodicity problems caused by the resulting very low probability of moving the trajectory, while in using the MD approach very short time steps are required making the simulations more computational time demanding. It was shown in Ref. [9] within the

*Electronic address: serge@physc.su.se

MC framework that after introducing just a few Fourier harmonics the number of required beads was quite substantially reduced.

A promising method to describe systems consisting of many identical particles was suggested by Miura and Okazaki [24]. They implemented a PIMD algorithm for systems of either fermionic or bosonic identical particles by introducing a pseudopotential between the beads taking into account the permutational symmetry. (A similar type of pseudopotential approach was also considered in Ref. [25].) However, these approaches again face problems at high number of beads. We, therefore, believe that the Bead-Fourier scheme is a realistic option to consider.

In this work, we use MD as a tool to generate a canonical ensemble of trajectories, not touching the question of a dynamical interpretation within the centroid dynamics. In this first preliminary study we apply our BF-PIMD method on two familiar quantum systems for which analytical exact solutions are available: harmonic potential (harmonic oscillator) and Coulombic potential with parameters corresponding to those for a hydrogen atom. Application of our method on systems with several identical particles will appear in subsequent publications.

The paper is organized as follows. The methodology, including a general formalism and its application on the chosen specific cases, are described in Sec. II. Simulation details are given in Sec. III. Results and discussion are presented in Sec. IV followed by conclusions in Sec. V. Some technical information is given in Appendix A.

II. THEORY

A. The Bead-Fourier approach

The basic idea behind the BF approach is to unite the Bead and Fourier approximations into a single scheme. We consider here quantum particle with a mass M confined in an external potential $V(x)$. In this section, all the formulas are derived for the one-dimensional case, since the generalization for the d-dimensional case is trivial. According to the work of Vorontsov-Velyaminov, Nesvit, and Gorbunov [9], the trajectory describing the particle can be presented as a number of beads, connected by continuous paths expressed as Fourier sine series:

$$x_j(\xi)=x_j+(x_{j+1}-x_j)\xi+\sum_{k=1}^{k_{\max}} a_{jk}\sin(k\pi\xi), \qquad (1)$$

where $k_{\max}$ is the maximum number of Fourier series terms, j and k are the indexes for the beads and Fourier harmonics, correspondingly. x_j are the bead coordinates and a_{jk} the Fourier amplitudes. Here, $x_j(\xi)$ describes the part of the trajectory between the beads j and $j+1$ in the imaginary time $\tau=j+\xi; 0<\xi<1$. Then, the partition function Z of the system can be written in the form [9]

$$Z=C(\beta)\int\prod_{j=1}^{n}\left(dx_j\prod_{k=1}^{k_{\max}}da_{jk}\right)\exp[-\beta H(x_j,a_{jk})], \quad (2)$$

where the effective Hamiltonian H is

$$H\{x_j,a_{jk}\}=\sum_{j=1}^{n}\left[\frac{Mn}{2\beta^2\hbar^2}\left((x_{j+1}-x_j)^2+\sum_{k=1}^{k_{\max}}\frac{(k\pi)^2}{2}a_{jk}^2\right)+\frac{1}{n}\int_0^1 d\xi V[x_j(\xi)]\right] \qquad (3)$$

and $C(\beta)$ is a normalization constant,

$$C(\beta)=\left(\frac{Mn}{2\beta\hbar^2}\right)^{(n/2)(1+k_{\max})}\frac{k_{\max}!}{\sqrt{2}}. \qquad (4)$$

In Eqs. (3) and (4), M is the particle mass, n is the number of beads, β is the inverse temperature ($\beta\equiv 1/kT$), and V is the potential energy of the system studied.

The classical object, isomorphic to the quantum particle is then a trajectory in the imaginary time, consisting of beads connected by harmonic springs (with the equilibrium distance equal to zero), while the interaction is distributed along the trajectory presented with $k_{\max}$ Fourier series terms in between the beads.

B. Canonical ensemble molecular dynamics by means of central mass Nosé-Hoover thermostating scheme

In the original formulation of the BF scheme [9], the system described by Hamiltonian (3) was sampled over the configurational space $\{x_j;a_{jk}\}$ using the MC method. In order to develop a path integral MD scheme, we treat Hamiltonian (3) as a potential energy and introduce the corresponding kinetic terms:

$$H\rightarrow H+\sum_{j=1}^{n}\left[\frac{p_j^2}{2m}+\sum_{k=1}^{k_{\max}}\frac{p_{jk}^2}{2m_k}\right]. \qquad (5)$$

Now we treat the bead coordinates $\{x_j\}$ and Fourier amplitudes $\{a_{jk}\}$ as generalized coordinates and $\{p_j;p_{jk}\}$ as the generalized momenta, conjugated to the bead coordinates and Fourier amplitudes, correspondingly. Then the Hamiltonian dynamics is applied in the phase space $\{x_j,p_j;a_{jk},p_{jk}\}$ with the bead mass m and the ''masses'' of the Fourier harmonics m_k. We use $m\equiv M/n$ in order to keep the mass of the whole object equal to the particle mass, though it is not necessary.

As our purpose is to generate a set of configurations for the system representing a canonical ensemble, we add the Nosé-Hoover thermostat chains to the Hamiltonian equations of motion, which can be done in a standard manner [26]. However, the results for the quantum harmonic oscillator were far from satisfactory. The classical Hamiltonian (3) in this case contains only harmonic terms and can be represented as a sum of n independent harmonic oscillators (normal modes). For the dynamics of a classical harmonic oscillator, there exists well-known ergodicity problem [27], making the standard single thermostat Nosé-Hoover procedure inapplicable [26]. Our further analysis showed that, e.g., results for the quantum mean energy were unstable depending on the initial conditions and the deviations of the average classical kinetic energy of the trajectory were up to 20%. The

system lacks ergodicity due to a very slow redistribution of the energy between global and internal movements. To correct this we therefore suggest independent thermostating of the mass center of the trajectory.

In the center-of-mass thermostating scheme the total momentum of the trajectory is thermostated as a separate degree of freedom, while the momenta of the beads are considered in the system of the mass center and thermostated as $n-1$ degrees of freedom. Thus, we apply two thermostat chains instead of one. The definitions of the internal and central mass momenta, respectively, are

$$p^c \equiv \sum_{j=1}^{n} p_j, \quad p_j^{int} \equiv p_j - \frac{p^c}{n}. \tag{6}$$

Following requirements should be satisfied:

$$\left\langle \frac{(p^c)^2}{mn} \right\rangle = k_B T, \tag{7}$$

$$\sum_{j=1}^{n} \left\langle \frac{(p_j^{int})^2}{m} \right\rangle = (n-1) k_B T, \tag{8}$$

where T is the temperature, k_B is the Boltzmann constant, and $\langle \cdots \rangle$ means the average over the MD simulation.

The Hamiltonian equations of motion together with thermostating of the bead coordinates are

$$\frac{\partial p^c}{\partial t} = \sum_{j=1}^{n} \frac{\partial p_j}{\partial t} - p^c \frac{\eta_1^c}{Q_1} = -\sum_{j=1}^{n} \frac{\partial H}{\partial x_j} - p^c \frac{\eta_1^c}{Q_1}, \tag{9}$$

$$\frac{\partial p_j^{int}}{\partial t} = \frac{\partial p_j}{\partial t} - \frac{1}{n}\frac{\partial p^c}{\partial t} - p_j^{int}\frac{\eta_1^{int}}{Q_1}$$

$$= -\frac{\partial H}{\partial x_j} + \frac{1}{n}\sum_{j=1}^{n}\frac{\partial H}{\partial x_j} - p_j^{int}\frac{\eta_1^{int}}{Q_1}, \tag{10}$$

$$\frac{\partial x_j}{\partial t} = \frac{\partial H}{\partial p_j} = \frac{p}{m}, \tag{11}$$

and for the Fourier amplitudes,

$$\frac{\partial p_{jk}}{\partial t} = -\frac{\partial H}{\partial a_{jk}} - p_{jk}\frac{\eta_{1k}}{Q_1}, \tag{12}$$

$$\frac{\partial a_{jk}}{\partial t} = \frac{\partial H}{\partial p_{jk}} = \frac{p_{jk}}{m_k}. \tag{13}$$

η_1 are Nosé thermosat momenta for the corresponding degrees of freedom, which are determined the same way as p_η in Ref. [26].

Here, we have implemented a separate thermostat chain for each set of Fourier harmonics with the same index k. Although not quite necessary the masses for all thermostat chains are chosen to be equal, as they work on objects with same masses. Note that Eqs. (11) and (13) for the bead velocities and Fourier amplitudes are uniform (they do not depend on the Hamiltonian).

The expressions for the energy estimators are given in Appendix A.

C. Quantum harmonic oscillator

Here we consider the one-dimensional case since the d-dimensional isotropic oscillator with a separate thermostat chain for each dimension is mathematically equivalent to d one-dimensional oscillators. The potential energy is

$$V[x_j(\xi)] = \frac{M\omega^2 x_j^2(\xi)}{2}. \tag{14}$$

Note that in the case of harmonic oscillator (14) the integral over ξ in Eq. (3) can be evaluated analytically, which is used in the formulas below.

For a harmonic oscillator it is useful to introduce intrinsic units in terms of inverse temperature β, frequency ω, and mass of the particle M. Thus, $\tilde{x} \equiv x/a_0$, $a_0 \equiv \sqrt{\hbar\omega/M\omega^2}$, $\tilde{H} \equiv H/\hbar\omega$, $\tilde{t} \equiv t\omega$. In intrinsic units, quantum oscillator can be characterized by a single parameter $b \equiv \beta\hbar\omega$.

Hamiltonian (3) in intrinsic units transforms to

$$\tilde{H} = \sum_{j=1}^{n} \frac{n}{2b^2}\left((\tilde{x}_{j+1} - \tilde{x}_j)^2 + \sum_{k=1}^{k_{\max}} \frac{(k\pi)^2}{2}\tilde{a}_{jk}^2 \right)$$

$$+ \frac{1}{n}\sum_{j=1}^{n} \int_0^1 d\xi \frac{\tilde{x}_j^{\,2}(\xi)}{2}. \tag{15}$$

After an analytical integration over the potential energy term in Eq. (3) the equations of motion with the Nosé-Hoover thermostat chains become [33]

$$\frac{\partial p^c}{\partial t} = -\sum_{j=1}^{n}\frac{1}{n}\left[x_j + \sum_{k=1}^{k_{\max}} \frac{[a_{jk} - (-1)^k a_{j-1,k}]}{k\pi} \right] - p^c\frac{\eta_1^c}{Q_1}, \tag{16}$$

$$\frac{\partial p_j^{int}}{\partial t} = -\frac{n}{b^2}(2x_j - x_{j+1} - x_{j-1}) - \frac{1}{n}\left[\frac{1}{6}(4x_j + x_{j+1} + x_{j-1}) + \sum_{k=1}^{k_{\max}} \frac{[a_{jk} + (-1)^{k+1} a_{j-1,k}]}{k\pi} \right]$$

$$+ \frac{1}{n^2}\left[\sum_{j=1}^{n} \left(x_j + \sum_{k=1}^{k_{\max}} \frac{[a_{jk} + (-1)^{k+1} a_{j-1,k}]}{k\pi} \right) \right]$$

$$- p_j^{int}\frac{\eta_1^{int}}{Q_1}. \tag{17}$$

Note that the sum of the internal forces in Eq. (17) should be zero, which can be easily proved using the properties of cyclic summation.

In the Results and Discussion section, our simulation results will be compared with the exact analytical expressions. The mean quantum energy of a harmonic oscillator in intrinsic units is [28]

$$\langle \tilde{H} \rangle = \frac{d}{2}\coth\left[\frac{b}{2}\right] \tag{18}$$

and its quantum coordinate distribution is given by

$$\rho(x)=(1-\exp[-b])\exp[-x^2]\sum_{n=1}^{\infty}|H_n(x)|^2\exp[-bn], \tag{19}$$

where $H_n(x)$ are the Hermite polynomials [28].

D. Hydrogen atom

Another realistic and analytically solvable quantum system is the hydrogen atom, presented as an electron in the Coulombic potential of a nucleus (proton). In order to avoid an infinite negative potential energy at zero distance, we change the Coulombic potential to a parabolic one at distances less than some cutoff radius r_0. The parameters of the potential inside the cutoff are fixed by the condition that the potential and its first derivative are continuous [9]:

$$V[r_j(\xi)]=\begin{cases}-\dfrac{e^2}{4\pi\varepsilon_0 r_j(\xi)}, & r_j(\xi)\geqslant r_0\\ \dfrac{e^2}{4\pi\varepsilon_0 r_0}\left(\dfrac{r_j^2(\xi)}{2r_0^2}-\dfrac{3}{2}\right), & r_j(\xi)\leqslant r_0,\end{cases} \tag{20}$$

where

$$r_j(\xi)=\sqrt{\sum_{i=1}^{3}x_{ij}^2(\xi)}. \tag{21}$$

Index i in Eqs. (20) and (21) runs over the three spatial coordinates. Other examples of smoothing potentials are presented, e.g., in Refs. [29,30]. The latter work is dedicated to the detailed analysis of the choice of the smoothing potential and its parameter.

In order to simplify the formulas we introduce the following notations:

$$C_1(T)\equiv\frac{nMk_B^2}{2\hbar^2}T^2, \quad C_2\equiv\frac{e^2}{4\pi\varepsilon_0 n}. \tag{22}$$

The potential energy now transforms into

$$\tilde{V}[r_j(\xi)]=\begin{cases}-\dfrac{1}{r_j(\xi)}, & r_j(\xi)\geqslant r_0\\ \dfrac{1}{r_0}\left(\dfrac{r_j^2(\xi)}{2r_0^2}-\dfrac{3}{2}\right), & r_j(\xi)\leqslant r_0,\end{cases} \tag{23}$$

while Hamiltonian (3), generalized to the three dimensions, is

$$H=\sum_{i=1}^{3}\left\{\sum_{j=1}^{n}\left[C_1(T)\left((x_{ij+1}-x_{ij})^2+\sum_{k=1}^{k_{\max}}\frac{(k\pi)^2}{2}a_{ijk}^2\right)+C_2\int_0^1 d\xi\tilde{V}[r_j(\xi)]\right]\right\}. \tag{24}$$

Since the integral in the potential part of Hamiltonian (24) cannot be evaluated analytically, it has to be calculated numerically in all formulas here, as well as further on. Before presenting the equations of motion with derivatives over the generalized coordinates we observe that

$$\frac{\partial V(\xi)}{\partial x_{ij}}=\frac{\partial V(\xi)}{\partial x_{ij}(\xi)}\frac{\partial x_{ij}(\xi)}{\partial x_{ij}}. \tag{25}$$

Following the scheme from the preceding section we write down the Hamiltonian equations of motion (starting from the case $r(\xi)\geqslant r_0$):

$$\frac{\partial p_i^c}{\partial t}=-C_2\sum_{j=1}^{n}\int_0^1 d\xi\frac{x_{ij}(\xi)}{r_j^3(\xi)}-p_i^c\frac{\eta_{1i}^c}{Q_1}, \tag{26}$$

$$\frac{\partial p_{ij}^{int}}{\partial t}=-C_1(T)[2x_{ij}-x_{ij-1}-x_{ij+1}]-C_2\left[\int_0^1 d\xi\frac{(1-\xi)x_{ij}(\xi)}{r_j^3(\xi)}+\int_0^1 d\xi\frac{\xi x_{ij-1}(\xi)}{r_{j-1}^3(\xi)}\right]+\frac{C_2}{n}\sum_{j=1}^{n}\int_0^1 d\xi\frac{x_{ij}(\xi)}{r_j^3(\xi)}-p_{ij}^{int}\frac{\eta_{1i}^{int}}{Q_1}. \tag{27}$$

The expression for the momenta conjugated with the Fourier amplitudes is

$$\frac{\partial p_{ijk}}{\partial t}=-C_1(T)(k\pi)^2a_{ijk}-C_2\int_0^1 d\xi\frac{\sin(k\pi\xi)x_{ij}(\xi)}{r_j^3(\xi)}-p_{ijk}\frac{\eta_{1ik}}{Q_1} \tag{28}$$

The thermostat chains are created for each dimension separately. Thus, there are $(k_{\max}+2)d$ thermostat chains in total.

If we consider the case $r\leqslant r_0$ all the expressions for the momenta and kinetic energy estimator will be the same after the substitution: $r_j(\xi)\to r_0$. The latter can be easily proved by using Eq. (25). The potential energy estimator should be considered separately, since it does not contain derivatives (see Appendix A).

In this work we only consider the electronic ground state of hydrogen atom. The analytical results for the energy and radial distribution function are [28]

$$E_{ground}=-hcR_H \tag{29}$$

$$\rho(r)=\frac{1}{\pi R_B^3}e^{-2r/R_B}, \tag{30}$$

where R_H is the Rydberg constant, R_B being the Bohr radius.

III. COMPUTATIONAL DETAILS

The time reversible molecular dynamics algorithm [31] with the Nosé-Hoover chains of three thermostats was implemented in all calculations. In fact, the effect of increasing the thermostat chains length from 2 to 3 is negligible. The same

chain length was found satisfactory in Ref. [14] for the *staging* algorithm.

In practical simulations of quantum harmonic oscillator, the simulation parameters are used in intrinsic units, chosen as time step $\delta t = 2 \times 10^{-3}$, thermostat masses $Q_2 = Q_3 = 0.01$, $Q_1 = nQ_2$, n being the number of beads [26]. Masses of the Fourier amplitudes were chosen as $m_k = 0.5k^{-1}$. This corresponds to an approximately equal fluctuation time for all Fourier amplitudes. Typical calculation consisted of 40 series 2×10^6 steps each. The statistical uncertainty of the quantum mean energy was within 0.5%.

For the hydrogen atom, the following units were used. Distances were measured in Å, time in femtoseconds, energies were converted to eV. Typical values for the simulations were time step $\delta t = 2 \times 10^{-3} fs$, cutoff radius $r_0 = 0.1$ Å. The thermostat masses were chosen to correspond to the thermostat fluctuation time of 1000 molecular dynamics time steps.

Numerical integration in the potential energy terms was carried out according to the trapezoidal rule with the number of integration steps around 10. The concrete number of the integration steps for the particular numbers of beads and Fourier harmonics could be chosen according to the data on the average distance between the beads and the curvature of the potential at this point.

For hydrogen atom, the simulations have been carried out at $T = 10^4$ K. Since the energy gap between the ground and the first excited state of the hydrogen is about 10 eV (above 10^5 K), the simulation temperature corresponds essentially to the ground state [9].

Typical calculation consisted of 40 series 5×10^5 steps each. The accuracy of the quantum energy was within 1%. It seems interesting that the accuracy remains constant either for harmonic oscillator or for hydrogen atom independently of the beads and Fourier harmonics numbers. Note that uncertainty for Coulombic potential was twice higher than for the harmonic oscillator, while the MD run was four times shorter.

IV. RESULTS AND DISCUSSION

A. Harmonic oscillator

We have carried out several tests that verify the correct work of the method. The first test concerns the proper work of the thermostats. In Fig. 1 the distributions of the classical momenta are compared with the analytical distributions:

$$\rho(p) = \sqrt{\frac{2\pi}{nb}} \exp\left[-\frac{nbp^2}{2} \right], \tag{31}$$

$$\rho(p_{int}) = \sqrt{\frac{2\pi(n-1)}{n^2 b}} \exp\left[-\frac{n^2 b p_{int}^2}{2(n-1)} \right], \tag{32}$$

$$\rho(p_c) = \sqrt{\frac{2\pi}{b}} \exp\left[-\frac{bp_c^2}{2} \right]. \tag{33}$$

Expressions (31)–(33) are given in intrinsic units. As it can be seen from Fig. 1(b), the simulation results are approaching the exact ones as the number of beads and Fourier harmonics is growing. In Fig. 1(a) we therefore present the ''worst'' case for the number of beads equal to 2 and only one Fourier harmonics. One can see that even in this case the simulation results nearly coincide with the analytical results. The deviation of the classical energies was also within the accuracy limit (data not shown). This demonstrates that the implemented thermostating scheme works properly.

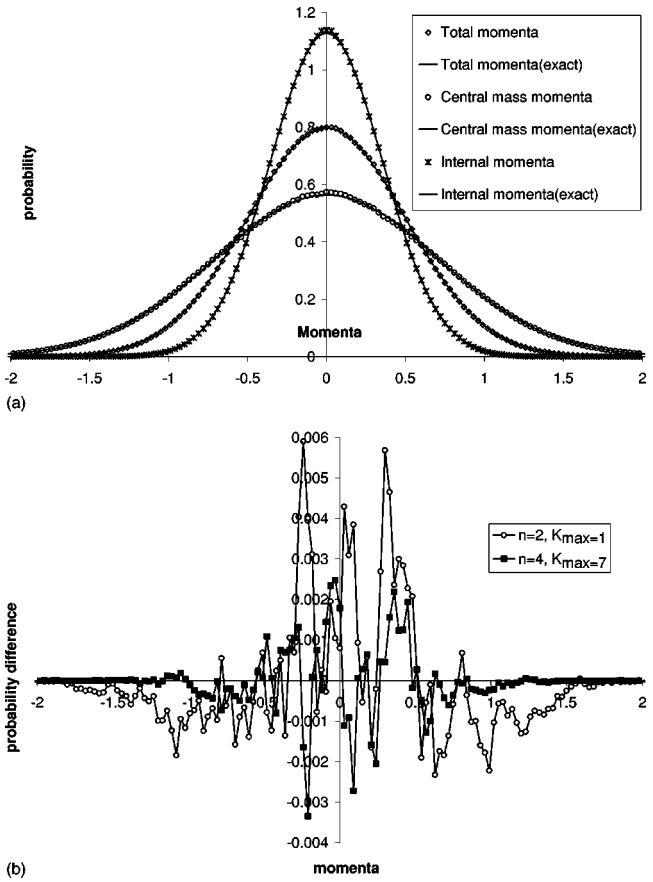

FIG. 1. The comparison of classical momentum distributions for quantum harmonic oscillator with corresponding analytical results. (a) The pairs of simulation results and analytical curves for total, internal, and mass centrum momenta. (b) The difference between simulation and analytical total momenta. Momenta are presented in intrinsic units.

The second test concerns the classical energy distributions obtained at different temperatures. It can be shown that such distributions should satisfy the relationship

$$\frac{\rho(E[b_1])}{\rho(E[b_2])} \exp[-(b_1 - b_2)E] = \text{Const} = \frac{\sinh[b_1/2]}{\sinh[b_2/2]}. \tag{34}$$

We simulated two temperatures $b_1 = 2.0$ and $b_2 = 2.2$ and obtained the classical energy distributions, both for the standard and for the center-of-mass thermostating schemes. The results are presented in Fig. 2. It is clear that results obtained via the center-of-mass thermostating scheme are much better than those obtained using the standard Hoover procedure.

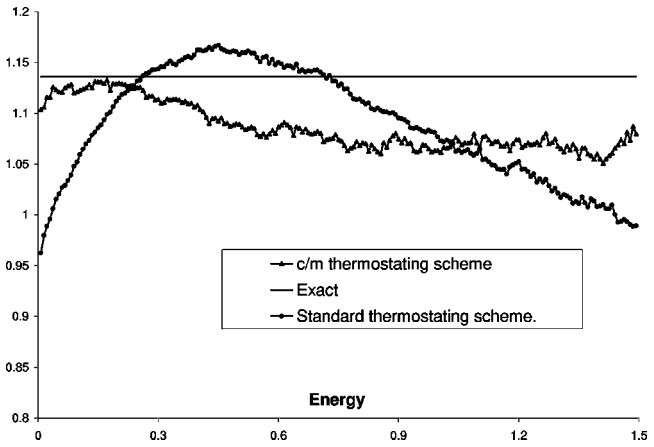

FIG. 2. Ratio (34) calculated for quantum harmonic oscillator $n=5$, $k_{\max}=0$ at two temperatures $b_1=2$ and $b_2=2.2$, for the standard and the center-of-mass thermostating schemes.

One can also conclude that the implemented center-of-mass thermostating scheme reproduces correctly the canonical ensemble.

The mean kinetic energy was evaluated using the virial estimator, which in the case of harmonic potential is identical to the potential energy estimator (see Appendix). That is why the total quantum energy was defined simply as twice the potential energy.

Two types of the potential energy estimators were used for the quantum mean energy (see Appendix). Using the first, ''continuous'' estimator, the potential energy is evaluated as an average of $V(x)$ over the whole trajectory [see Eq. (A2) in the Appendix]. According to the second, ''pure bead'' estimator, the averaging is taken only over bead points disregarding the trajectory in between (A13) and (A15). Somewhat counterintuitively, we discovered that the use of ''pure bead'' estimators within the Bead-Fourier MD scheme provides a better convergence relative to the number of beads (see Fig. 3, Table I). There is, however, a reasonable explanation for that. If one considers the numerical evaluation of the integral of x^2 using the trapezoidal rule (analog of the pure bead estimator), it will always be greater than its exact

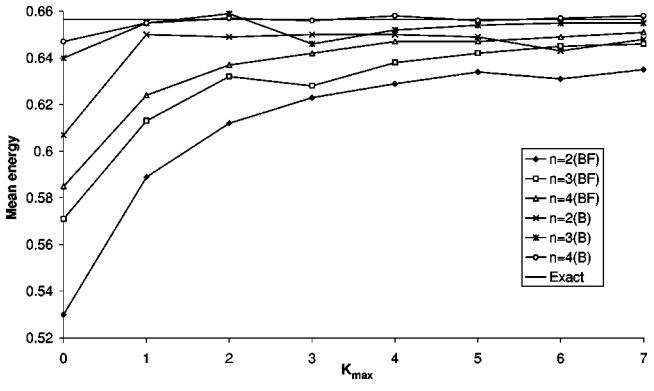

FIG. 3. The mean energy for quantum harmonic oscillator at $b=2$ for various numbers of beads and Fourier harmonics obtained via ''continuous'' and ''pure bead'' estimators. Energies are in intrinsic units.

TABLE I. Quantum mean energy for harmonic oscillator at $b=2$ for various numbers of beads n and Fourier harmonics $k_{\max}$. The first row in each cell corresponds to ''continuous'' estimators, while the second corresponds to ''pure bead'' estimators. Energies are presented in intrinsic units.

	Number of beads, n		
$k_{\max}$	2	3	4
0	0.530	0.571	0.585
	0.607	0.640	0.647
1	0.589	0.613	0.624
	0.650	0.655	0.655
2	0.612	0.632	0.637
	0.649	0.659	0.657
3	0.623	0.628	0.642
	0.650	0.646	0.656
4	0.629	0.638	0.647
	0.650	0.652	0.658
5	0.634	0.642	0.647
	0.649	0.654	0.656
6	0.631	0.645	0.649
	0.643	0.655	0.657
7	0.635	0.646	0.651
	0.648	0.655	0.658

value (the continuous estimator). Since in the finite-bead approximation of path integrals the potential energy is underestimated, we have a clear case of cancellation of errors in using the pure bead estimator. Situation may be different in the case of convex potential functions (with negative second derivative), but these are not typical cases. Important is also that both the estimators provide exact values at large number of beads.

Analysis of data in Table I shows that addition of a few Fourier harmonics already improves the precision quite considerably. For example, for the number of beads $n=3$, already one single Fourier harmonic was enough to give the exact energy value within statistical error, using pure bead energy estimators. The use of Bead-Fourier approach is clearly beneficial in comparison to the pure bead method. Another advantage of the Bead-Fourier scheme is that the ergodicity problem, especially severe for the harmonic potential within the pure bead scheme and related to the weak interaction of harmonic modes, is intrinsically solved by artificial ''interactions'' between beads and Fourier harmonics (10) and (12).

The results for the quantum coordinate distributions are presented in Fig. 4. We obtained two types of the distributions: one was calculated from the bead positions, while the other was evaluated from the whole trajectory, i.e., including the parts of the trajectory in between the beads. Since the quantum mean energy can be calculated from the quantum coordinate distribution, the former corresponds to *pure* bead energy estimators and the latter corresponds to the *continuous* estimators (see Appendix A). Note that already for the number of beads $n=2$ and with only one single Fourier harmonics the bead coordinate distribution nearly coincides

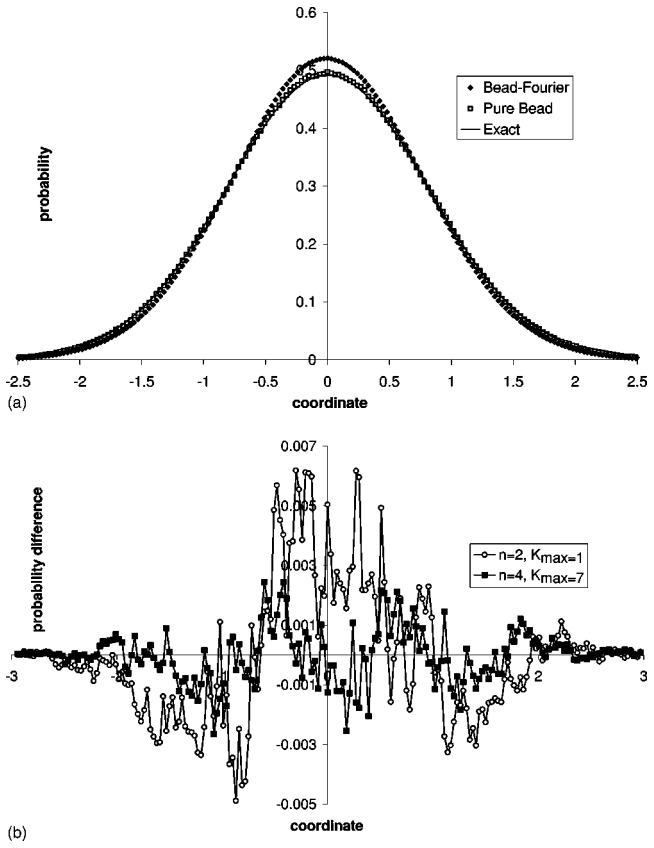

FIG. 4. The quantum coordinate distribution for harmonic oscillator at $b=2$. (a) Comparison between the results obtained via ''continuous'' and ''pure bead'' estimators and the analytical ones for $n=2$, $k_{\max}=1$. (b) The differences between two quantum coordinate distributions for $n=2$, $k_{\max}=1$; $n=4$, $k_{\max}=7$ and the analytically exact distribution. Distances are given in intrinsic units.

with the exact one, while the deviations of the coordinate distribution built on the whole trajectory are relatively big. This latter fact illustrates that the averages calculated over beads only are better than those calculated over the whole trajectory. We should stress, however, that in both the cases the dynamics was created by the Bead-Fourier scheme, i.e., forces acting on beads depend on the whole trajectory. Again, the pure bead dynamics yields worse results; moreover, it suffers from ergodicity problems.

The data presented above correspond to a weakly degenerated system. Now, let us consider a strongly degenerated case with $b=15.8$. Such system can be compared with OH-bond vibrations at room temperature. The results for the quantum mean energy for a different number of beads and Fourier components are presented in Fig. 5. For instance, for the number of beads $n=5$ any number of Fourier harmonics $k_{\max}\geqslant 2$ gives results inside the statistical error. Within the pure bead algorithm, it would be necessary to take several hundred beads to reach the same precision. In Ref. [14], $n=400$ was used to simulate a harmonic oscillator at this temperature and the *staging* algorithm was applied to sample the big number of bead degrees of freedom in this system. The accuracy achieved in Ref. [14] either by staging MD or MC was about the same (0.3%) as in our work.

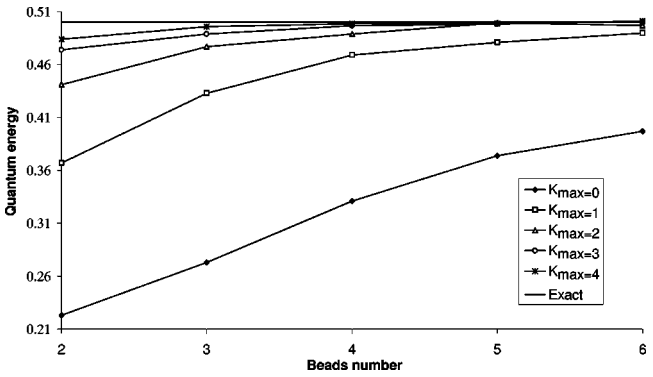

FIG. 5. Quantum harmonic oscillator at $b=15.8$. The dependences of the quantum mean energy (in intrinsic units) over beads numbers for various numbers of Fourier harmonics. Comparison with the exact result.

Note also that although the number of beads and Fourier harmonics have to be increased as b is growing, the increased CPU time is somewhat compensated by the possibility to increase the size of the MD time step, since the stiffness of the springs is proportional to n/b^2.

B. Hydrogen atom

Following the line of the preceding section we start from the classical momenta distributions (Fig. 6). Classical momenta should be always (for any potential energy) distributed according to the Maxwell distribution and this comparison serves as a test that the MD algorithm reproduces a canonical ensemble. Deviations from the exact result are shown in Fig. 6(b). One can see that these deviations are one order of magnitude smaller than in the case case of harmonic potential [Fig. 1(b)]). The reason is that the simulations of the Coulomb potential with hydrogen atom parameters require more beads than the harmonic oscillator, while the deviations of momenta from Maxwell distribution decrease with the increasing number of beads.

The results for the quantum mean energy for the hydrogen atom are presented in Fig. 7 and Table II. Note that as it was in the case of the quantum harmonic oscillator, the average energies obtained by pure bead estimators converge faster than those obtained by using Bead-Fourier estimators, although the difference is smaller here. One can also see a very clear improvement of the results after addition of the Fourier harmonics. The same effect exists for quantum coordinate distributions, shown in Fig. 8. In the case of the Coulombic potential the improvement of the distribution due to inclusion of the Fourier harmonics is even more pronounced than in the case of harmonic oscillator.

These results demonstrate that without Fourier harmonics the method is unable to yield reasonable results even for extended numbers of beads, n. At small n, the beads get easily stacked near the nucleus due to the strong attraction. Without a finite cutoff of potential (20), the beads simply collapse on the nucleus. As a result, at zero Fourier components and a few dozens of beads, the potential energy is several times lower than the exact value. Addition of a few

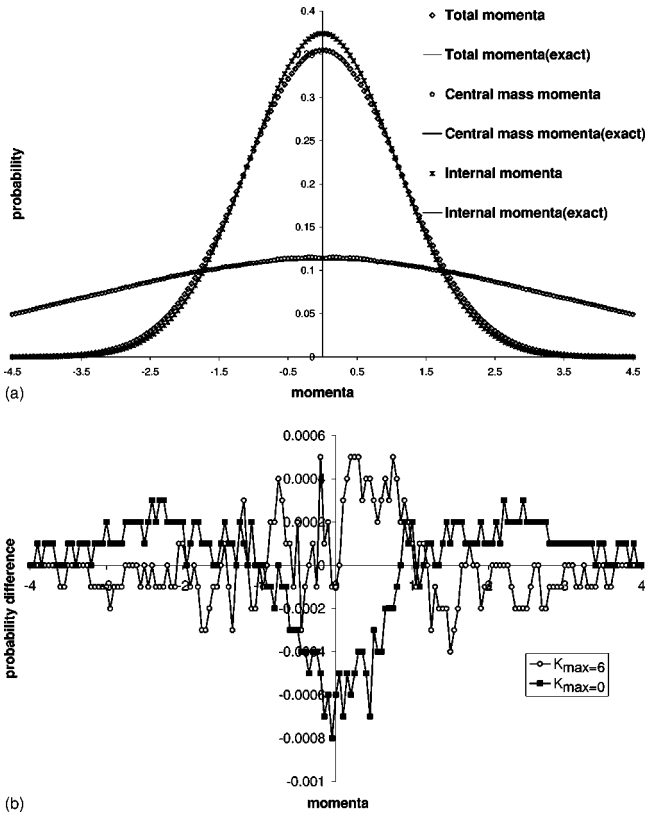

FIG. 6. The comparison of classical momenta distributions for hydrogen atom with the analytical results. (a) The pairs of simulation results and analytical curves for total, internal, and mass centrum momenta. (b) The difference between simulation and analytical total momenta.

(5–6) Fourier components allows to reach 1% precision with no more than 30 beads.

Table III contains information about the average distances between the beads for different numbers of beads and Fourier harmonics. It is known that when the finite-bead approximation is sufficient, this distance should scale as $n^{-1/2}$. One can see that this dependence more or less holds when

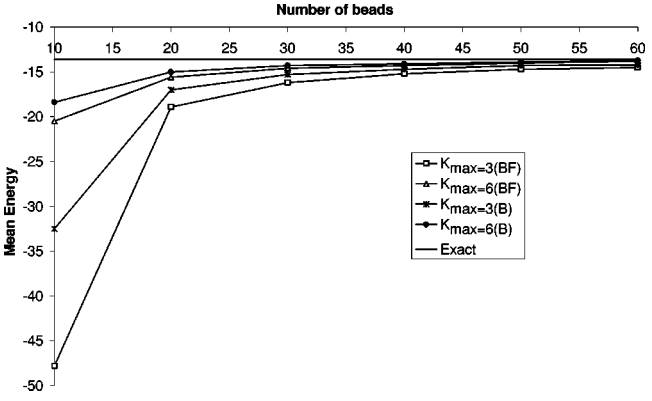

FIG. 7. The dependences of the quantum mean energy (eV) for hydrogen atom on the beads number for numbers of Fourier harmonics 3 and 6 obtained using ''continuous'' and ''pure bead'' estimators.

TABLE II. Quantum mean energy (eV) for hydrogen atom presented for various numbers of beads n and Fourier harmonics $k_{\max}$. The first row in each cell corresponds to ''continuous'' estimators, while the second corresponds to ''pure bead'' estimators.

	Number of beads, n					
$k_{\max}$	10	20	30	40	50	60
0	−189.8	−161.4	−116.7	−59.1	−35.3	−27.2
	−171.6	−132.9	−91.4	−47.5	−29.7	−23.7
1	−161.6	−54.2	−25.5	−19.8	−17.8	−16.8
	−125.0	−39.4	−21.3	−17.7	−16.4	−15.7
2	−114.2	−24.0	−18.2	−16.4	−15.6	−15.1
	−76.2	−20.0	−16.5	−15.4	−14.9	−14.6
3	−47.8	−18.9	−16.2	−15.2	−14.7	−14.5
	−32.5	−17.0	−15.3	−14.7	−14.3	−14.2
4	−28.4	−17.2	−15.5	−14.7	−14.4	−14.2
	−22.3	−15.9	−14.8	−14.2	−14.1	−14.0
5	−22.9	−16.2	−15.0	−14.5	−14.1	−14.1
	−19.5	−15.4	−14.6	−14.1	−13.9	−13.9
6	−20.5	−15.6	−14.6	−14.3	−14.0	−13.8
	−18.4	−15.0	−14.3	−14.1	−13.9	−13.7

the number of Fourier components is 5 or 6. For a smaller number of Fourier components (and especially for $k_{\max}=0$) the opposite trend occurs with the average distance being smaller for smaller n. This results from strong attractions pulling the trajectory closer to the nucleus in the Coulombic potential well. Addition of Fourier components, even at small n, leads to an increase of the average distance up to a limiting value, corresponding to the case when the trajectory correctly describes the electron density around the hydrogen atom.

V. CONCLUSION

Bead-Fourier path-integral formulation of molecular dynamics method is presented. In this first paper we have tested the BF-PIMD method for both quantum harmonic oscillator and hydrogen atom and demonstrated that it accurately re-

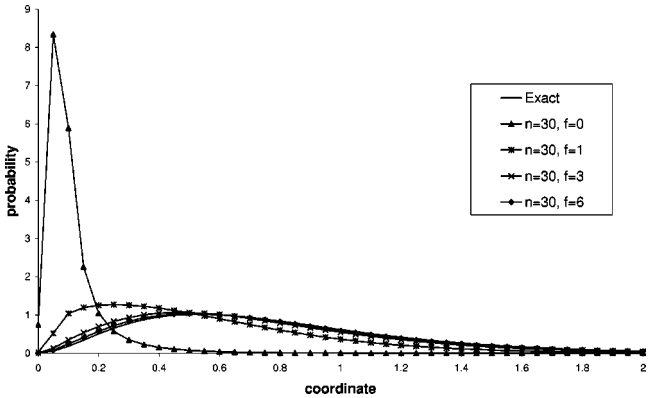

FIG. 8. The quantum coordinate distributions for hydrogen atom with $n=30$ and various numbers of Fourier harmonics. Comparison with the analytical result. Distances are given in Å.

TABLE III. Average distances (Å) between the beads for hydrogen atom for various numbers of beads n and Fourier harmonics $k_{\max}$.

	Number of beads, n					
$k_{\max}$	10	20	30	40	50	60
0	0.0270	0.0414	0.0750	0.1462	0.1714	0.1717
1	0.0373	0.1736	0.2196	0.2113	0.1976	0.1850
2	0.0919	0.2513	0.2376	0.2178	0.2008	0.1871
3	0.2154	0.2668	0.2425	0.2198	0.2021	0.1877
4	0.2735	0.2729	0.2445	0.2213	0.2027	0.1880
5	0.2941	0.2760	0.2453	0.2214	0.2031	0.1883
6	0.3044	0.2784	0.2465	0.2221	0.2032	0.1886

produces the properties for which there exist analytical solutions. For the pure bead method the center-of-mass thermostating scheme already reduces the ergodicity problem, yielding much more stable results compared to the standard thermostating scheme. Finally, introduction of Fourier harmonics eliminates the ergodicity problem completely. The averages obtained, using the Bead-Fourier molecular dynamics with pure bead estimators, converge to the exact result faster than those calculated along the trajectories.

Comparison of the simulation results with the exact data obtained analytically shows that after introducing only few (often even one single) Fourier harmonics considerably improves the results even for a small number of beads. The combined Bead-Fourier method shows a clear improvement compared to the pure bead or pure Fourier schemes. Using the BF-PIMD algorithm, the computing time per time step is roughly proportional to the product of the number of beads and the maximum number of Fourier terms. The optimal ratio between the numbers of beads and Fourier harmonics depends from on the system studied. Although we have not done any precise benchmarking, our simulation times show that, e.g., for hydrogen the best results are obtained when the number of beads is several times (5–10) larger than the corresponding number of Fourier harmonics.

ACKNOWLEDGMENT

The work was supported by the Swedish Research Council (Vetenskapsrådet).

APPENDIX: ENERGY ESTIMATORS

The estimators of the mean kinetic and potential energies can be obtained from the Gibbs-Helmholtz equation:

$$\langle H\rangle = \frac{\partial}{\partial\beta}(\beta F) = -\frac{\partial \ln Z}{\partial\beta} = -\left\langle \frac{1}{C(\beta)}\frac{\partial C(\beta)}{\partial\beta}\right\rangle + \left\langle \frac{\partial(\beta U_{kin})}{\partial\beta}\right\rangle + \left\langle \frac{\partial(\beta U_{pot})}{\partial\beta}\right\rangle \equiv \langle E_{kin}\rangle + \langle E_{pot}\rangle, \tag{A1}$$

where the potential energy [34] is

$$\langle E_{pot}\rangle = \sum_{j=1}^{n}\left\langle \frac{1}{n}\int_0^1 d\xi V[x_j(\xi)]\right\rangle \tag{A2}$$

and the kinetic energy is

$$\langle E_{kin}^{prim}\rangle = \frac{n}{2\beta}(1+k_{\max}) - \left\langle \sum_{j=1}^{n}\frac{Mn}{2\beta^2\hbar^2}\left[(x_{j+1}-x_j)^2 + \sum_{k=1}^{k_{\max}}\frac{(k\pi)^2}{2}a_{jk}^2\right]\right\rangle. \tag{A3}$$

The latter result is called *primitive estimator* [3]. Note that it does not depend on the potential. It is known that the uncertainty of the primitive estimator is large and grows with the number of beads [32]. Another estimator without this disadvantage called *virial* estimator has been suggested [32]:

$$\langle E_{kin}^{vir}\rangle = \frac{1}{2n}\left\langle \hat{L}\sum_{j=1}^{n}\int_0^1 d\xi V[x_j(\xi)]\right\rangle, \tag{A4}$$

where

$$\hat{L} \equiv \sum_{j=1}^{n}\left[x_j\frac{\partial}{\partial x_j} + \sum_{k=1}^{k_{\max}} a_{jk}\frac{\partial}{\partial a_{jk}}\right]. \tag{A5}$$

We have mainly used the latter for the kinetic energy.

For the quantum harmonic oscillator the expressions for energy estimators are

$$\langle E_{kin}^{vir}\rangle = \left\langle \sum_{j=1}^{n}\left\{\frac{1}{12n}[4x_j^2 + x_jx_{j+1} + x_jx_{j-1}] + \frac{1}{2n}\sum_{k=1}^{k_{\max}}\left[\frac{x_j[a_{j,k}-(-1)^k a_{j-1,k}]}{k\pi} + \frac{a_{jk}^2}{2} + \frac{a_{j,k}[x_j-(-1)^k x_{j+1}]}{k\pi}\right]\right\}\right\rangle, \tag{A6}$$

$$\langle E_{pot}\rangle = \sum_{j=1}^{n}\frac{1}{n}\left[\frac{1}{6}(x_{j+1}^2 + x_{j+1}x_j + x_j^2) + \sum_{k=1}^{k_{\max}}\frac{[x_j-(-1)^k x_{j+1}]a_{jk}}{k\pi} + \sum_{k=1}^{k_{\max}}\frac{a_{jk}^2}{4}\right]. \tag{A7}$$

Note that according to the virial theorem, Eqs. (A6) and (A7) must be equal. In fact, they are, that can be proved using the properties of cycling summations.

In the case of the hydrogen atom the expressions for the energy estimators are as follows. The kinetic part remains unchanged, and we write down the primitive estimator in the appropriate units:

$$\langle E_{kin}^{prim}\rangle = \frac{dn}{2}k_B T(1+k_{\max}) - \left\langle \sum_{i=1}^{d}\left\{\sum_{j=1}^{n} C_1(T)\left[(x_{i,j+1}-x_{i,j})^2 + \sum_{k=1}^{k_{\max}}\frac{(k\pi)^2}{2}a_{ijk}^2\right]\right\}\right\rangle, \tag{A8}$$

d being the dimensionality. The potential energy estimator

$$\langle E_{pot}\rangle = \frac{C_2}{n}\left\langle \sum_{j=1}^{n}\int_0^1 d\xi \tilde{V}_{eff}[r_j(\xi)]\right\rangle. \tag{A9}$$

Then obtaining the virial estimator is straightforward:

$$\langle E_{kin}^{vir}\rangle = \frac{C_2}{2n}\left\langle \hat{L}\sum_{j=1}^{n}\int_0^1 d\xi \tilde{V}_{eff}[r_j(\xi)]\right\rangle, \tag{A10}$$

where

$$\hat{L} \equiv \sum_{i=1}^{3}\sum_{j=1}^{n}\left[x_{ij}\frac{\partial}{\partial x_{ij}} + \sum_{k=1}^{k_{\max}} a_{ijk}\frac{\partial}{\partial a_{ijk}}\right], \tag{A11}$$

$$\langle E_{kin}^{vir}\rangle = \frac{C_2}{n}\left\langle \sum_{i=1}^{3}\sum_{j=1}^{n}\int_0^1 d\xi\left[x_{ij}\left\{\frac{(1-\xi)x_{ij}(\xi)}{r_j^3(\xi)} + \frac{\xi x_{ij-1}(\xi)}{r_{j-1}^3(\xi)}\right\} + \sum_{k=1}^{k_{\max}}\frac{a_{ijk}\sin(k\pi\xi)x_{ij}(\xi)}{r_j^3(\xi)}\right]\right\rangle. \tag{A12}$$

Expressions above correspond to ''continuous'' estimators in which the averaging is made along the trajectory. As we discussed in the text, another possibility is to calculate the averages from the beads positions only removing the parts of the trajectory in between. The expressions for the mean energies in this case are

$$\langle E_{kin}^{vir}\rangle = \langle E_{pot}\rangle = \sum_{j=1}^{n}\frac{x_j^2}{2n}, \tag{A13}$$

for harmonic oscillator, and

$$\langle E_{kin}^{vir}\rangle = \frac{C_2}{2}\sum_{i=1}^{3}\sum_{j=1}^{n}\left[\frac{x_{ij}^2}{r_j^3(0)}\right], \tag{A14}$$

for hydrogen atom. The potential estimator can be obtained directly:

$$\langle E_{pot}\rangle = \begin{cases} -C_2\sum_{i=1}^{3}\sum_{j=1}^{n}\frac{x_{ij}^2}{r_j^3(0)}, & r_j(\xi)\geqslant r_0 \\ \frac{C_2}{2r_0}\cdot\sum_{j=1}^{n}\left[\frac{r_j^2(0)}{r_0^2}-3\right], & r_j(\xi)\leqslant r_0. \end{cases} \tag{A15}$$

[1] R.P. Feynman and A.R. Hibbs, *Quantum Mechanics and Path Integrals* (McGraw-Hill, New York, 1965).
[2] R.P. Feynman, *Statistical Mechanics* (Addison-Wesley, Redwood City, CA 1972).
[3] J.A. Barker, J. Chem. Phys. **70**, 2914 (1979).
[4] J.D. Doll and D.L. Freeman, J. Chem. Phys. **80**, 2239 (1984).
[5] S.L. Mielke and D.G. Truhlar, J. Chem. Phys. **114**, 621 (2001).
[6] R.D. Coalson, J. Chem. Phys. **85**, 926 (1986).
[7] R.D. Coalson, D.L. Freeman, and J.D. Doll, J. Chem. Phys. **91**, 4242 (1989).
[8] C. Chakravarty, M.C. Gordillo, and D.M. Ceperley, J. Chem. Phys. **109**, 2123 (1998); J.D. Doll and D.L. Freeman, *ibid.* **111**, 7685 (1999); C. Chakravarty, M.C. Gordillo, and D.M. Ceperley, *ibid.* **111**, 7687 (1999).
[9] P.N. Vorontsov-Velyaminov, M.O. Nesvit, and R.I. Gorbunov, Phys. Rev. E **55**, 1979 (1997).
[10] P.N. Vorontsov-Velyaminov, R.I. Gorbunov, and S.D. Ivanov, Comput. Phys. Commun. **121**, 64 (1999).
[11] P.N. Vorontsov-Velyaminov and R.I. Gorbunov, Contrib. Plasma Phys. **42**, 27 (2000).
[12] B. de Raedt, L.M. Sprik, and M.L. Klein, J. Chem. Phys. **80**, 5719 (1984).
[13] R.W. Hall and B.J. Berne, J. Chem. Phys. **81**, 3641 (1984).
[14] M.E. Tuckerman, B.J. Berne, G.J. Martyna, and M.L. Klein, J. Chem. Phys. **99**, 2796 (1993).
[15] M. Parinello and A. Rahman, J. Chem. Phys. **80**, 860 (1984).
[16] J. Cao and G.A. Voth, J. Chem. Phys. **99**, 10070 (1994).
[17] J. Cao and G.A. Voth, J. Chem. Phys. **100**, 5093 (1994); **100**, 5106 (1994).
[18] J. Cao and G.A. Voth, J. Chem. Phys. **101**, 6157 (1994); **101**, 6168 (1994).
[19] M.E. Tuckerman, D. Marx, M.L. Klein, and M. Parrinello, J. Chem. Phys. **104**, 5579 (1995).
[20] U.W. Schmitt and G.A. Voth, J. Chem. Phys. **111**, 9361 (1999).
[21] J. Poulsen, S.R. Keiding, and P. Rossky, J. Chem. Phys. Lett. **336**, 488 (2001).
[22] Q. Shi and E. Geva, J. Chem. Phys. **116**, 3223 (2002).
[23] J. Hutter *et al.*, CPMD, IBM Zurich Research Laboratory and MPI für Festkrperförchung 1995–2002.
[24] S. Miura and S. Okazaki, J. Chem. Phys. **112**, 10 116 (2000).
[25] A.P. Lyubartsev and P.N. Vorontsov-Velyaminov, Phys. Rev. A **48**, 4075 (1993).
[26] G.J. Martyna, M.L. Klein, and M. Tuckerman, J. Chem. Phys. **97**, 2635 (1992).
[27] W.G. Hoover, Phys. Rev. A **31**, 1695 (1985).
[28] P.W. Atkins, *Physical Chemistry*, 6th ed. (Oxford University Press, Oxford, 1998).

[29] A. Monnier, V. Srdanov, G. Stucky, and H. Metiu, J. Chem. Phys. **100**, 6944 (1994).
[30] M.H. Müser and B.J. Berne, J. Chem. Phys. **107**, 571 (1997).
[31] M. Tuckerman, B.J. Berne, and G.J. Martyna, J. Chem. Phys. **97**, 1990 (1992).
[32] M.F. Herman, E.J. Bruskin, and B.J. Berne, J. Chem. Phys. **76**, 5150 (1982).
[33] From now on we omit the tildes for the variables expressed in the intrinsic units.
[34] All equations are written for one-dimensional case.